J|A|C|S
ARTICLES
Published on Web 12/14/2005

Gold Nanoclusters Protected by Conformationally Constrained Peptides

Laura Fabris,[‡] Sabrina Antonello,[‡] Lidia Armelao,[§] Robert L. Donkers,[‡] Federico Polo,[‡] Claudio Toniolo,[‡] and Flavio Maran*,[‡]

Contribution from the Department of Chemistry, University of Padova, via Marzolo 1, 35131 Padova, Italy, and Department of Chemistry, ISTM-CNR, via Marzolo, 1, 35131 Padova, Italy

Received September 10, 2005; E-mail: f.maran@chfi.unipd.it

Abstract: The preparation and properties of a series of gold nanoclusters protected by thiolated peptides based on the α-aminoisobutyric acid (Aib) unit are described. The peptides were devised to form 0−3 C═O···H−N intramolecular hydrogen bonds, as required by their 3_{10}-helical structure. The monolayer-protected clusters (MPCs) were prepared, using a modified version of the two-phase Brust−Schiffrin preparation, and fully characterized with ^{1}H NMR spectrometry, IR and UV−vis absorption spectroscopies, transmission electron microscopy (TEM), thermogravimetric analysis (TGA), and X-ray photoelectron spectroscopy (XPS). The MPCs were obtained with core diameters in the range of 1.1−2.3 nm, depending on the reaction conditions. Structured peptides formed smaller clusters. The smallest MPC obtained is in agreement with the average formula $Au_{38}Pep_{18}$. The results showed that the chemical integrity of the peptide is maintained upon monolayer formation and that the average number of peptide ligands per gold cluster is typically 75−85% the value calculated for alkanethiolate MPCs of similar sizes. The IR and NMR spectra indicated that in the monolayer the peptides are involved in both intra- and interligand C═O···H−N hydrogen bonds.

Introduction

Understanding and controlling the physical and chemical properties of monolayer-protected gold clusters (MPCs) is an active area of current research.[1,2] The MPCs are rather easily fabricated and possess high stability.[2,3] The protecting ligands provide a way to decorate the outer MPC shell with molecular groups to carry out specific functions, which is an issue of paramount relevance for the use of these nanosystems as devices and sensors.[1−4] Exploiting MPCs for applied purposes thus requires a proper control of the properties of the ligands employed, which are usually thiolate adsorbates. Monolayer formation on gold substrates is driven by the chemical bonding between the sulfur and gold atoms and by interactions between neighboring adsorbate molecules. Such a driving force controls the properties and stability of monolayers protecting small metal clusters (3D architectures) as well as those of self-assembled monolayers (SAMs) on extended (2D) metal surfaces. Alkanethiolates are often employed to make SAMs, and thus the adsorbates interact mainly through intermolecular van der Waals forces. Additional interactions, however, may enhance the stability of SAMs, such as intermolecular C═O···H−N hydrogen bonding between embedded amide groups, as found with various 2D SAMs.[5] Peptides are thus expected to be particularly convenient molecules to use, also in view of their intrinsic relevance for biological applications. A variety of strategies to prepare peptide 2D SAMs has been reported, where oligopeptides are usually modified by introducing thiol groups at either the N- or C-terminus.[6] Generally, peptide monolayers are well-packed, and their stability may be strengthened by C═O···H−N

[‡] Department of Chemistry, University of Padova.
[§] Department of Chemistry, ISTM-CNR.

(1) (a) Zhang, J. Z.; Wang, Z.; Liu, J.; Chen, S.; Liu, G. *Self-Assembled Nanostructures*; Kluwer Academic/Plenum: New York, 2003. (b) Schmid, G. *Nanoparticles*; Wiley-VCH: Weinheim, Germany, 2004. (c) El-Sayed, M. A. *Acc. Chem. Res.* **2001**, *34*, 257−264.
(2) (a) Templeton, A. C.; Wuelfing, W. P.; Murray, R. W. *Acc. Chem. Res.* **2000**, *33*, 27−36. (b) Schmid, G.; Corain, B. *Eur. J. Inorg.* **2003**, 3081−3098. (c) Daniel, M.-C.; Astruc, D. *Chem Rev.* **2004**, *104*, 293−346.
(3) Brust, M.; Kiely, C. J. *Colloids Surf., A* **2002**, *202*, 175−186.
(4) (a) Jahn, W. *J. Struct. Biol.* **1999**, *127*, 106−112. (b) Shipway, A. N.; Katz, E.; Willner, I. *ChemPhysChem* **2000**, *1*, 18−52. (c) Shenhar, R.; Rotello, V. *Acc. Chem. Res.* **2003**, *36*, 549−561. (d) *Nanobiotechnology: Concepts, Applications and Perspective*; Niemeyer, C. M., Mirkin, C. A., Eds.; Wiley-VCH: Weinheim, Germany, 2004. (e) Katz, E.; Willner, I. *Angew. Chem., Int. Ed.* **2004**, *43*, 6042−6108.
(5) (a) Nuzzo, R. G.; Dubois, L. H.; Allara, D. L. *J. Am. Chem. Soc.* **1990**, *112*, 558−569. (b) Lenk T. J.; Hallmark, V. M.; Hoffmann, C. L.; Rabolt, J. F.; Castner, D. G.; Erdelen, C.; Ringsdorf, H. *Langmuir* **1994**, *10*, 4610−4617. (c) Wagner, P.; Hegner, M.; Guntherodt, H.-J.; Semenza, G. *Langmuir* **1995**, *11*, 3867−3875. (d) Tam-Chang, S. W.; Biebuyck, H. A.; Whitesides, G. M.; Jeon, N.; Nuzzo, R. G. *Langmuir* **1995**, *11*, 4371−4382. (e) Clegg, R. S.; Hutchison, J. E. *Langmuir* **1996**, *12*, 5239−5243. (f) Clegg, R. S., Reed, S. M.; Hutchison, J. E. *J. Am. Chem. Soc.* **1998**, *120*, 2486−2487. (g) Sabapathy, R. C.; Bhattacharyya, S.; Leavy, M. C.; Cleland, W. E., Jr.; Hussey, C. L. *Langmuir* **1998**, *14*, 124−136. (h) Zhang, J.; Zhang, H. L.; Chen, M.; Zhao, J.; Liu, Z. F.; Li, H. L. *Ber. Bunsen-Ges. Phys. Chem.* **1998**, *102*, 701−703. (i) Clegg, R. S.; Hutchison, J. E. *J. Am. Chem. Soc.* **1999**, *121*, 5319−5327. (j) Valiokas, R.; Svedhem, S.; Svensson, S. C. T.; Liedberg, B. *Langmuir* **1999**, *15*, 3390−3394. (k) Clegg, R. S.; Reed, S. M.; Smith, R. K.; Barron, B. L.; Rear, J. A.; Hutchison, J. E. *Langmuir* **1999**, *15*, 8876−8883. (l) Smith, R. K.; Reed, S. M.; Lewis, P. A.; Monnell, J. D.; Clegg, R. S.; Kelly, K. F.; Bumm, L. A.; Hutchison, J. E.; Weiss, P. S. *J. Phys. Chem. B* **2001**, *105*, 1119−1122. (m) Valiokas, R.; Svedhem, S.; Östblom, M.; Svensson, S. C. T.; Liedberg, B. *J. Phys. Chem. B* **2001**, *105*, 5459−5469. (n) Lewis, P. A.; Smith, R. K.; Kelly, K. F.; Bumm, L. A.; Reed, S. M.; Clegg, R. S.; Gunderson, J. D.; Hutchison, J. E.; Weiss, P. S. *J. Phys. Chem. B* **2001**, *105*, 10630−10636. (o) Valiokas, R.; Östblom, M.; Svedhem, S.; Svensson, S. C. T.; Liedberg, B. *J. Phys. Chem. B* **2002**, *106*, 10401−10409. (p) Petoral, R. M.; Uvdal, K. *J. Phys. Chem. B* **2003**, *107*, 13396−13402. (q) Inman, C. E.; Reed, S. M.; Hutchison, J. E. *Langmuir* **2004**, *20*, 9144−9150.
(6) Wen, X.; Linton, R. W.; Formaggio, F.; Toniolo, C.; Samulski, E. T. *J. Phys. Chem. A* **2004**, *108*, 9673−9681.

 10.1021/ja0560581 CCC: $33.50

interchain hydrogen bonds. Similar issues are expected to affect the stability of SAMs formed on small gold clusters, although for them the radial distribution of the ligands makes the interchain distance a subtle function of the distance from the core as well as of the core size and geometry.[7]

Several studies have been carried out on gold nanoparticles protected by peptides, particularly in connection to possible biomedical applications.[4e,8] The core diameters employed are generally larger than 10 nm, and thus the properties of the particles resemble those of the bulk material; few investigations concern MPCs in the size region marking the transition to the molecular-like behavior (1−2 nm). Murray and co-workers described the synthesis of tiopronin MPCs (down to 1.8 nm size) and their modification through ligand place exchange to prepare nanoparticles displaying redox and fluorophoric properties.[9] Peptide backbones have been added onto preformed MPCs by ligand place exchange[10] or multistep synthesis.[11] In addition to place exchange, mixed monolayers based on tiopronin or glutathione ligands were shown to directly form under controlled conditions.[12] It has also been reported that large gold nanoparticles can be prepared by using the amino acid itself as the reductant.[13] Glutathione MPCs proved to be a particularly efficient ligand to passivate gold nucleation to very limited amounts of atoms, yielding molecule-like particles displaying interesting optical properties.[14] Metal nanoparticles protected by single amino acids or linear peptides showed a subtle dependence of size and stability on the metal/ligand combination.[15] Interesting studies for applications in the area of nuclear targeting are also worth mentioning, in which gold nanoclusters are capped by suitable peptides for crossing cellular membranes.[16] Amino acids and peptides are also useful to create complex assemblies of nanoparticles[17] and to form stable functionalized gold nanoparticles for molecular recognition.[8,18]

As opposed to the SAMs formed on extended surfaces, the radial orientation of the thiolate ligands in small MPCs make their outer terminals prone to lateral motion. These fluctuations increase the possibility that exogenous species, such as solvent or electrolytes, could penetrate the capping monolayer, which for some applications might be quite unsought. In this paper, we describe the results of a study aimed at preparing gold clusters protected by peptides displaying a definite conformational preference and thus remarkable stiffness. We used a series of structurally well-defined peptide systems based on the α-aminoisobutyric acid (Aib) residue. The Aib homooligomers are characterized by marked steric hindrance at the α-carbon, resulting in restricted torsional freedom.[19,20] Consequently, they are significantly rigid even when they are short,[21] which is a general feature shared by oligopeptides based on C^{α}-tetrasubstituted α-amino acids.[19,20] It is worth stressing that this 3D-structural propensity is not encountered with peptide systems based on coded α-amino acids, which start to form helices only for rather long oligomers.[22] Instead, the tendency of Aib homopeptides to form β-turns and 3_{10}-helices starts from the tripeptide.[20] In the 3_{10}-helix, each intramolecular C═O···H−N hydrogen bond involves residues i and $i + 3$ and a single helical turn requires 3.24 amino acid residues,[21b] while the α-helix is characterized by a pitch of 3.63 residues/turn. Formation of the 3_{10}-helix is accompanied by the onset of a strong oriented dipole moment that develops along the peptide backbone.[23] As opposed to simple alkanethiols, for which the increase in the number of methylene units increases the flexibility of the ligand, the key motif of the selected peptides is that the increase of the number of units is accompanied by a concomitant increase of the number of intramolecular hydrogen bonds and thus of the peptide stiffness. This feature and, particularly, the unique relative rigidity of short Aib homopeptides are being successfully exploited as spacers or templates in electrochemical and spectroscopic investigations.[24−26] Since 2D or 3D SAM formation already causes the conformational freedom of alkanethiols to decrease dramatically, we expected that for the same reason our peptides would have behaved as even more rigid ligands.

In this paper, we describe the synthesis, characterization, and properties of peptide MPCs having average core diameters ranging from 1.1 to 2.3 nm. We used the thiolated peptides **0**−**3**, where the number of amino acids is such to allow forming structures characterized by zero, one, two, or three intramolecular C═O···H−N hydrogen bonds, respectively.

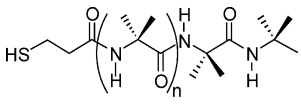

0-3

(7) (a) Hostetler, M. J.; Stokes, J. J.; Murray, R. W. *Langmuir* **1996**, *12*, 3604−3612. (b) Boal, A.; Rotello, V. M. *Langmuir* **2000**, *16*, 9527−9532.
(8) Rosi, N. L.; Mirkin, C. A. *Chem. Rev.* **2005**, *105*, 1547−1562.
(9) (a) Templeton, A. C.; Chen, S.; Gross, S. M.; Murray, R. W. *Langmuir* **1999**, *15*, 66−76. (b) Templeton, A. C.; Cliffel, D. E.; Murray, R. W. *J. Am. Chem. Soc.* **1999**, *121*, 7081−7089. (c) Huang, T.; Murray, R. W. *Langmuir* **2002**, *18*, 7077−7081.
(10) (a) Pengo, P.; Broxterman, Q. B.; Kaptein, B.; Pasquato, L.; Scrimin, P. *Langmuir* **2003**, *19*, 2521−2524. (b) Lévy, R.; Thanh, N. T. K.; Doty, C.; Hussain, I.; Nichols, R. J.; Schiffrin, D. J.; Brust, M.; Fernig, D. G. *J. Am. Chem. Soc.* **2004**, *126*, 10076−10084.
(11) (a) Templeton, A. C.; Hostetler, M. J.; Warmoth, E. K.; Chen, S.; Hartshorn, C. M.; Krishnamurthy, V. M.; Forbes, M. D. E.; Murray, R. W. *J. Am. Chem. Soc.* **1998**, *120*, 4845−4849. (b) Fan, J.; Chen, S.; Gao, Y. *Colloid Surf., B* **2003**, *28*, 199−207. (c) Sung, K.-M.; Mosley, D. W.; Peelle, B. R.; Zhang, S.; Jacobson, J. M. *J. Am. Chem. Soc.* **2004**, *126*, 5064−5065.
(12) Zheng, M.; Huang, X. *J. Am. Chem. Soc.* **2004**, *126*, 12047−12054.
(13) (a) Selvakannan, P. R.; Mandal, S.; Phadtare, S.; Gole, A.; Pasricha, R.; Sastry, M. *Langmuir* **2003**, *19*, 3545−3549. (b) Bhargava, S. K.; Booth, J. M.; Agrawal, S.; Coloe, P.; Kar, G. *Langmuir* **2005**, *21*, 5949−5956.
(14) (a) Schaaff, T. G.; Knight, G.; Shafigullin, M. N.; Borkman, R. F.; Whetten, R. L. *J. Phys. Chem. B* **1998**, *102*, 10643−10646. (b) Schaaff, T. G.; Whetten, R. L. *J. Phys. Chem. B* **2000**, *104*, 2630−2641. (c) Link, S.; El-Sayed, M. A.; Schaaff, T. G.; Whetten, R. L. *Chem. Phys. Lett.* **2002**, *356*, 240−246. (d) Link, S.; Beeby, A.; FitzGerald, S.; El-Sayed, M. A.; Schaaff, T. G.; Whetten, R. L. *J. Phys. Chem. B* **2002**, *106*, 3410−3415. (e) Negishi, Y.; Takasugi, Y.; Sato, S.; Yao, H.; Kimura, K.; Tsukuda, T. *J. Am. Chem. Soc.* **2005**, *126*, 6518−6519. (f) Negishi, Y.; Nobusada, K.; Tsukuda, T. *J. Am. Chem. Soc.* **2005**, *127*, 5261−5270.
(15) Slocik, J. M.; Wright, D. W. *Biomacromolecules* **2003**, *4*, 1135−1141.
(16) (a) Tkachenko, A. G.; Xie, H.; Coleman, D.; Glomm, W.; Ryan, J.; Anderson, M. F.; Franzen, S.; Feldheim, D. L. *J. Am. Chem. Soc.* **2003**, *125*, 4700−4701. (b) Xie, H.; Tkachenko, A. G.; Glomm, W. R.; Ryan, J.; Brennaman, M. K.; Papanikolas, J. M.; Franzen, S.; Feldheim, D. L. *Anal. Chem.* **2003**, *75*, 5797−5805. (c) Tkachenko, A. G.; Xie, H.; Liu, Y.; Coleman, D.; Ryan, J.; Glomm, W. R.; Shipton, M. K.; Franzen, S.; Feldheim, D. L. *Bioconjugate Chem.* **2004**, *15*, 482−490.
(17) (a) Wong, M. S.; Cha, J. N.; Choi, K.-S.; Deming, T. J.; Stucky, G. D. *Nano Lett.* **2002**, *2*, 583−587. (b) Chakrabarti, R.; Klibanov, A. M. *J. Am. Chem. Soc.* **2003**, *125*, 12531−12540. (c) Stevens, M. M.; Flynn, N. T.; Wang, C.; Tirrell, D. A.; Langer, R. *Adv. Mater.* **2004**, *16*, 915−918. (d) Zhong, Z.; Subramanian, A. S.; Highfield, J.; Carpenter, K.; Gedanken, A. *Chem. Eur. J.* **2005**, *11*, 1473−1478.
(18) Wang, Z.; Lévy, R.; Fernig, D. G.; Brust, M. *Bioconjugate Chem.* **2005**, *16*, 497−500.
(19) Karle, I.; Balaram, P. *Biochemistry* **1990**, *29*, 6747−6756.
(20) Toniolo, C.; Crisma, M.; Formaggio, F.; Peggion, C. *Biopolymers (Pept. Sci.)* **2001**, *60*, 396−419.
(21) (a) Toniolo, C.; Bonora, G. M.; Barone, V.; Bavoso, A.; Benedetti, E.; Di Blasio, B.; Grimaldi, P.; Lelj, F.; Pavone, V.; Pedone, C. *Macromolecules* **1985**, *18*, 895−902. (b) Toniolo, C.; Benedetti, E. *Trends Biochem. Sci.* **1991**, *16*, 350−353.
(22) Goodman, M.; Toniolo, C.; Pallai, P. In *Forum Peptides*; Castro, B., Martinez, J., Eds.; Dhor: Nancy, France, 1985; pp 146−174.
(23) Shin, Y.-G.; Newton, M. D.; Isied, S. S. *J. Am. Chem. Soc.* **2003**, *125*, 3722−3732.

The MPC synthesis follows a modified version of the two-phase preparation described by Brust et al.[27] and commonly used for the production of aryl and alkanethiolate coated MPCs. The clusters were characterized by ^{1}H NMR spectrometry, IR and UV−vis absorption spectroscopies, transmission electron microscopy (TEM), thermogravimetric analysis (TGA), and X-ray photoelectron spectroscopy (XPS). Our results indicate that a rigid peptide structure is maintained in the monolayer as well as in the free ligand. By altering the ratio of the Au(III) salt and capping thiol, the core diameter of the cluster could be varied down to 1.1 nm, in agreement with the formation of Au_{38} clusters, which were recently prepared using phenylethanethiolate and hexanethiolate as the ligands.[28] Spectral data indicated that the peptides are involved in both intra- and interligand C═O···H−N hydrogen bonds, resulting in densely packed monolayers.

Experimental Section

Chemicals. All chemicals were commercially available and used as received. The syntheses of peptide precursors and ligands are described in detail in the Supporting Information. All peptides were stable and could be stored at low temperature for months. The synthesis of additional peptides, having general formula $CH_3CO-(Aib)_n-NHtBu$, was carried out as previously reported.[25c]

Synthesis of Peptide-Coated MPCs. A general procedure for the preparation of the crude reaction product of the **3**-protected gold nanocluster using a 3:1 thiol-to-Au ratio at 0 °C is described. After adding 0.102 g (0.26 mmol) of $HAuCl_4{\cdot}(H_2O)_3$ in 10 mL of water to a solution of 0.403 g (0.74 mmol) of tetra-*n*-octylammonium bromide (Oct_4NBr) in 25 mL of toluene in a 250 mL flask, the mixture was stirred for 15 min until the water phase changed from yellow to colorless and the toluene layer from colorless to a dark red. The aqueous layer was removed, the organic phase was dehydrated with Na_2SO_4, and 0.375 g (0.75 mmol) of **3** was added in 5 mL of methanol with stirring. After 5 min, the solution became colorless (if the synthesis is carried out using a 0.5:1 thiol-to-Au ratio, the color does not disappear completely), signaling reaction of the gold salt with the thiol to form a soluble polymeric AuSR compound. The reaction was carried out for 30 min, and then the flask was cooled to 0 °C in an ice water bath. Then, 0.100 g (2.7 mmol) of $NaBH_4$, dissolved in 5 mL of methanol and cooled on ice, were added to the polymeric AuSR solution under vigorous stirring. A black color, indicative of MPC formation, was immediately produced in the solution mixture and a gas evolved. The reaction temperature was maintained at 0 °C in the ice bath and the mixture vigorously stirred for 2 h, after which the flask content was poured into 40 mL of water and then extracted after addition of 20 mL of methylene chloride. The organic extracts were dried over Na_2SO_4, filtered, and evaporated, providing a brown solid. The MPC was separated from most unreacted peptide thiol and peptide disulfide by dissolving the MPC in 5 mL of acetone, leaving a white precipitate behind, and filtering on a fine fritted glass filter. Residual peptide impurities were removed by collecting the MPC in the filtrate, evaporating the acetone, and repeating the acetone wash (2 mL). Purification of each MPC was different, depending on the specific peptide, and is described in the Supporting Information.

Infrared Absorption Spectroscopy. Both the solid-state (KBr disk technique) and solution (CH_2Cl_2, using cells having 1 mm optical path and CaF_2 windows) IR absorption spectra were recorded with a Perkin-Elmer model 1720X FT-IR spectrophotometer, nitrogen-flushed, equipped with a sample-shuttle device, at 2 cm^{-1} nominal resolution, and averaging 100 scans.

UV−Vis Absorption Spectroscopy. UV−vis spectra were taken in methanol and CH_2Cl_2 solutions with a Varian Cary 5 UV−vis spectrophotometer. The MPC concentrations were chosen to provide an optical absorbance A near 400 nm of ∼1.0. The experiments were carried out at room temperature, the absorption spectra were recorded from 300 to 1500 nm, and the contribution of the background was accounted for.

^{1}H Nuclear Magnetic Resonance Spectroscopy. ^{1}H NMR spectra were obtained by using a Bruker model AC 200 spectrometer, a Bruker model Avance 300 spectrometer, a Bruker model AM 400 spectrometer, or a Bruker model Avance 600 instrument. Deuteriochloroform (99.96%, *d*; Acros Organics), deuterated acetonitrile (99.95%, d_3; Acros Organics), deuterated methanol (99.8%, d_4; Acros Organics), and deuterated dimethyl sulfoxide (99%, d_6; Aldrich) were used as the solvents. Chemical shifts (δ) are reported as parts per million (ppm) downfield from tetramethylsilane. Two-dimensional spectra were obtained from ROESY experiments carried out in deuteriochloroform and CD_3CN.

Thermogravimetric Analysis. TGA was performed with a TA Instruments SDT 2960 system on accurately weighed, carefully dried, 1−8 mg cluster samples, under N_2 and in standard Al pans. In the temperature ramp (25−600 °C at 15 °C/min.), the organic volatilization and ensuing mass loss occurred for all samples at temperatures above 200 °C, leaving a gold metal residue in the pan.

Transmission Electron Microscopy. TEM phase contrast images were obtained with a JEOL JEM 2010 microscope operating at 200 keV. The MPC samples were prepared by spreading a droplet of 1 mg/mL MPC in methylene chloride, methanol, or ethanol on standard carbon-coated (20−30 nm) Formvar films on copper grids (400 mesh). To analyze a statistically significant number of particles (usually 100−130), three regions were typically imaged for each sample in the 100−250 K magnification range. The core sizes were quantified on the digitized photographic images by using the Photoshop Elements software; values from obvious twins or aggregates of particles were discarded. The histograms were obtained by using Scion Image Beta Release 2. The dispersity data will refer to the standard deviations (σ); the average deviations are ∼20% smaller than the σ values.

X-ray Photoelectron Spectroscopy. XPS analyses were performed with a Perkin-Elmer Φ 5600-ci spectrometer using non-monochromatized (15 kV, 400 W) Mg Kα radiation (1253.6 eV). The appropriate gold cluster solution, in ethanol or dichloromethane, was drop-cast onto a platinum substrate. The carefully dried sample was mounted on a steel sample holder and introduced directly, by a fast-entry lock system, into the XPS analytical chamber. The sample analysis area was 800 μm in diameter, and the working pressure was $<5 \times 10^{-8}$ Pa. The spectrometer was calibrated assuming the binding energy (BE) of the

(24) Toniolo, C.; Crisma, M.; Formaggio, F.; Peggion, C.; Broxterman, Q. B.; Kaptein, B. *Biopolymers (Pept. Sci.)* **2004**, *76*, 162−176.
(25) (a) Antonello, S.; Formaggio, F.; Moretto, A.; Toniolo, C.; Maran, F. *J. Am. Chem. Soc.* **2003**, *125*, 2874−2875. (b) Improta, R.; Antonello, S.; Formaggio, F.; Maran, F.; Rega, N.; Barone, V. *J. Phys. Chem. B* **2005**, *109*, 1023−1033. (c) Polo, F.; Antonello, S.; Formaggio, F.; Toniolo, C.; Maran, F. *J. Am. Chem. Soc.* **2005**, *127*, 492−493.
(26) (a) Hanson, P.; Millhauser, G.; Formaggio, F.; Crisma, M.; Toniolo, C. *J. Am. Chem. Soc.* **1996**, *118*, 7618−7625. (b) Polese, A.; Mondini, S.; Bianco, A.; Toniolo, C.; Scorrano, G.; Guldi, D. M.; Maggini, M. *J. Am. Chem. Soc.* **1999**, *121*, 3446−3452. (c) Pispisa, B.; Stella, L.; Venanzi, M.; Palleschi, A.; Viappiani, C.; Polese, A.; Formaggio, F.; Toniolo, C. *Macromolecules* **2000**, *33*, 906−915. (d) Pispisa, B.; Stella, L.; Venanzi, M.; Palleschi, A.; Polese, A.; Formaggio, F.; Toniolo, C. *J. Pept. Res.* **2000**, *56*, 298−306. (e) Pispisa, B.; Mazzuca, C.; Palleschi, A.; Stella, L.; Venanzi, M.; Wakselman, M.; Mazaleyrat, J.-P.; Rainaldi, M.; Formaggio, F.; Toniolo, C. *Chem. Eur. J.* **2003**, *9*, 4084−4093. (f) Sartori, E.; Toffoletti, A.; Rastrelli, F.; Corvaja, C.; Bettio, A.; Formaggio, F.; Oancea, S.; Toniolo, C. *J. Phys. Chem. A* **2003**, *107*, 6905−6912. (g) Sartori, E.; Toffoletti, A.; Corvaja, C.; Moroder, L.; Formaggio, F.; Toniolo, C. *Chem. Phys. Lett.* **2004**, *385*, 362−367. (h) Venanzi, M.; Valeri, A.; Palleschi, A.; Stella, L.; Moroder, L.; Formaggio, F.; Toniolo, C.; Pispisa, B. *Biopolymers (Biospectroscopy)* **2004**, *75*, 128−139.
(27) Brust, M.; Walker, M.; Bethell, D.; Schiffrin, D. J.; Whyman, R. *J. Chem. Soc., Chem. Commun.* **1994**, 801−802.
(28) (a) Lee, D.; Donkers, R. L.; DeSimone, J. M.; Murray, R. W. *J. Am. Chem. Soc.* **2003**, *125*, 1182−1183. (b) Lee, D.; Donkers, R. L.; Wang, G.; Harper, A. S.; Murray, R. W. *J. Am. Chem. Soc.* **2004**, *126*, 6193−6199. (c) Donkers, R. L.; Lee, D.; Murray, R. W. *Langmuir* **2004**, *20*, 1945−1952. (d) Jimenez, V. L.; Georganopoulou, D. G.; White, R. J.; Harper, A. S.; Mills, A. J.; Lee, D.; Murray, R. W. *Langmuir* **2004**, *20*, 6864−6870. (e) Wang, G.; Huang, T.; Murray, R. W.; Menard, L.; Nuzzo, R. G. *J. Am. Chem. Soc.* **2005**, *127*, 812−813.

$Au4f_{7/2}$ line at 83.9 eV with respect to Fermi level. The standard deviation for the BE values was 0.2 eV. A low-energy flood gun was used to minimize charge when necessary. The residual BE shifts (on the order of 0.4−0.6 eV) were corrected by assigning to the C1s peak associated with the methyl groups a value of 285.0 eV. Survey scans were run in the 0−1100 eV range (pass energy, 187.85 eV), while detailed scans were recorded for the Au4f, C1s, O1s, N1s, and S2p regions. The analyses involved Shirley-type background subtraction[29] and, whenever necessary, spectral deconvolution, which was carried out by nonlinear least-squares curve fitting, adopting a Gaussian−Lorentzian sum function. The atomic composition of the drop-cast MPC samples was calculated by peak integration, using the sensitivity factors supplied by the spectrometer manufacturer and taking into account the geometric configuration of the apparatus.

Results and Discussion

Synthesis, Characterization, and Properties of the Peptide Ligands. The syntheses of peptide ligands **0**−**3** were carried out as follows. The *tert*-butyl amides of the *Z*-protected peptides, (*Z* = benzyloxycarbonyl) *Z*-$(Aib)_n$−NH*t*Bu, were obtained by condensation of *Z*-Aib−OH[30] with the appropriate H−$(Aib)_{n-1}$−NH*t*Bu segments. Carboxyl activation was achieved by use of the EDC/HOAt method.[31] The N^{α}-deprotected peptides, obtained by catalytic hydrogenation of the *Z*-$(Aib)_n$−NH*t*Bu oligomers, were converted to their $Ph_3C-S-(CH_2)_2-CO-(Aib)_n-NHtBu$ analogues, compounds **0a**−**3a**, by reaction with $Ph_3C-S-(CH_2)_2-COOH$. Finally, the triphenylmethyl (trityl) sulfides were treated with trifluoroacetic acid and triisopropylsilane to yield the corresponding thiols.

FT-IR absorption spectra of **0a**−**3a** and **0**−**3** were obtained in CH_2Cl_2, which is a solvent of low polarity having no propensity to behave as a hydrogen-bond acceptor, and the analysis focused on the N−H and C═O stretching modes. The N−H stretching region (amide A, 3450−3250 cm^{-1}) is composed by a high-energy region corresponding to the NH groups that are not involved in hydrogen bonds and a low-energy region pertaining to NH groups involved in hydrogen bonds.[21a] As one passes from **0** to **3** (or, similarly, from **0a** to **3a**), the low-energy N−H stretching band appears starting from **1** and **1a**, which are the shortest peptides for which formation of an incipient 3_{10}-helix is possible.[32] As the peptide chain length increases, the frequency of the N−H stretching band of intramolecularly H-bonded peptides decreases, which is a marker of the increase of peptide stiffness.[21a] In a previous IR absorption study, we could show that Aib homooligomers with 3−5 NH groups (such as peptides **1**−**3** and **1a**−**3a** in this work) are characterized by 41, 69, and 80% of intramolecular H-bonds of the 3_{10}-helix type, respectively.[21a] These data highlight the great efficiency of the Aib unit in stabilizing folded and helical species even in very short peptides, but also explain the broadness of the IR bands (the spectra will be illustrated later, in Figure 7, in comparison with those obtained for the corresponding peptide MPCs), which result from a combination of contributions from multiple conformations. This conclusion is confirmed by the number and position of the high-resolution enhanced bands exhibited by Aib homooligomers with 5 NH groups.[33]

Bidimensional ^{1}H NMR spectra were obtained from ROESY experiments carried out in $CDCl_3$ and CD_3CN (Supporting Information, Figure S1). Through-space connectivities of the $C^{\beta}H(i-1)\rightarrow NH(i)$ type (between the methyl protons of an Aib and the amide proton of the following residue) and $NH(i)\rightarrow NH(i+1)$ type were used for the assignment of the proton resonances. The rather intense $NH(i)\rightarrow NH(i+1)$ cross-peak signals obtained for **1a** suggest that even this short peptide adopts a prevailing folded structure (β-turn).[34] The same outcome is observed with **3a**. Noteworthy, the same conformation is kept unaltered in both $CDCl_3$ and CD_3CN, the latter solvent being an appreciable H-bond acceptor. To test the participation of the amide protons in intramolecular hydrogen bonds, the ^{1}H NMR spectra of **1a** and **3a** were obtained in the 3D structure supporting solvent $CDCl_3$ and their evolution was studied as a function of the addition of the good H-bond acceptor Me_2SO-d_6.[21a] The N(1)H proton of both peptides was found to be very sensitive to Me_2SO-d_6 addition, the peaks shifting to lower fields. A similar but less pronounced behavior was observed for the N(2)H proton, while the other amide protons were essentially insensitive. A similar outcome was observed with the corresponding $CH_3CO-(Aib)_n-NHtBu$ peptides, which rules out a possible involvement of the sulfur atom in the secondary structure. This trend is in line with the normal behavior of Aib homopeptides for which the sensitivity of the N(1)H protons is notably higher than that of the N(2)H protons.[21a] The absence of effects brought about on the other NH protons points to the failure of Me_2SO-d_6 to disrupt the intramolecular H-bonds involving them. Since in the 3_{10}-helix the formation of stable intramolecular H-bonds starts from the N(3)H proton, we infer that these peptides adopt such an ordered secondary structure.

Preparation of Peptide MPCs. Peptides **0**−**3** are soluble in many organic solvents, and thus the MPCs could be prepared by using a procedure similar to that reported by Brust et al. at 0 °C.[27] We focused on two thiol concentrations, at 3:1 and 0.5:1 ratios to the gold salt. Details are provided in the Experimental Section and in the Supporting Information. The MPC syntheses generally led to materials with a narrow range of core diameters, in line with the best results obtained in MPC syntheses based on alkanethiolate ligands.[9a,35−38] This tendency and the fact that separation from unreacted peptide is easily performed by taking advantage of solubility differences are useful features that make the MPC purification procedure rather straightforward.

The TEM analysis was employed to determine the average MPC size and to test the sensitivity of the preparation procedure on experimental parameters. Similarly to previous reports of alkanethiolate MPCs,[35] we found that decreasing the temperature

(29) Shirley, D. A. *Phys. Rev. B* **1972**, *55*, 4709−4714.
(30) (a) McGahren W. J.; Goodman, M. *Tetrahedron* **1967**, *23*, 2017−2030. (b) Valle, G.; Formaggio, F.; Crisma, M.; Bonora, G. M.; Toniolo, C.; Bavoso, A.; Benedetti, E.; Di Blasio, B.; Pavone, V.; Pedone, C. *J. Chem. Soc., Perkin Trans. 2* **1986**, 1371−1376. (c) Leplawy, M. T.; Jones, D. S.; Kenner, G. W.; Sheppard, A. C. *Tetrahedron* **1960**, *11*, 29−51.
(31) Carpino, L. A. *J. Am. Chem. Soc.* **1993**, *115*, 4397−4398. EDC = 1-(3-dimethyl-aminopropyl)-3-ethylcarbodiimide; HOAt = 1-hydroxy-7-aza-1,2,3-benzotriazole.
(32) We also found that the investigated peptides do not display any appreciable tendency to self-aggregate in solution, e.g., by head-to-tail intermolecular hydrogen bonding, even at concentrations as large as 10 mM.
(33) Kennedy, D. F.; Crisma, M.; Toniolo, C.; Chapman, D. *Biochemistry* **1991**, *30*, 6541−6548.
(34) Wüthrich, K. In *NMR of Proteins and Nucleic Acids*; Wiley: New York, 1986; pp 192−196.
(35) Hostetler, M. J.; Wingate, J. E.; Zhong, C.-J.; Harris, J. E.; Vachet, R. W.; Clark, M. R.; Londono, J. D.; Green, S. J.; Stokes, J. J.; Wignall, G. D.; Glish, G. L.; Porter, M. D.; Evans, N. D.; Murray, R. W. *Langmuir* **1998**, *14*, 17−30.
(36) Shimmin, R. G.; Schoch, A. B.; Braun, P. V. *Langmuir* **2004**, *20*, 5613−5620.
(37) (a) Chen, S.; Murray, R. W. *Langmuir* **1999**, *15*, 682−689. (b) Shon, Y.-S.; Gross, S. M.; Dawson, B.; Porter, M.; Murray, R. W. *Langmuir* **2000**, *16*, 6555−6561.
(38) Zheng, M.; Li, Z.; Huang, X. *Langmuir* **2004**, *20*, 4226−4235.

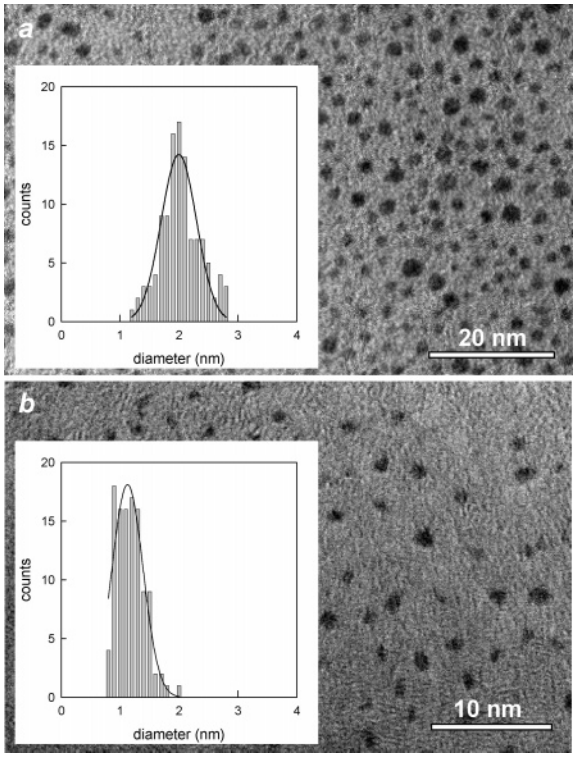

Figure 1. TEM images of **2**-MPC obtained from preparations at (a) 0.5:1 S:Au ratio and (b) 3:1 S:Au ratio. Insets show histograms of the corresponding distribution of core sizes.

Table 1. MPC Core Diameters Determined from TEM Images or Extrapolated from Analysis of the Derivative of the UV−Vis Absorption Spectra

peptide	S:Au[a]	d_{TEM}[b] (nm)	d_{UV}(2.10eV)[c] (nm)	d_{UV}(2.65eV)[c] (nm)
0	0.5:1	2.3(0.6)	2.2	2.3
1		1.8(0.4)	1.8	1.7
2		2.0(0.3)	2.2	2.1
3		1.9(0.4)	2.1	1.9
0	3:1	1.8(0.2)	1.7	1.8
1		1.3(0.3)	1.2	1.3
2		1.1(0.2)	1.2	1.1
3		1.3(0.3)	1.2	1.3

[a] $T = 0$ °C. [b] The number in parentheses is the standard deviation (dispersity). [c] From a correlation between the derivative of absorbance and the TEM diameters (see text).

reduces the average core diameter (d). For example, the 0.5:1 preparations of **3**-MPC at room temperature and 0 °C yield average d values of 2.1 and 1.9 nm, respectively. In the search for suitable conditions to prepare small peptide MPCs, all syntheses described below were thus carried out at 0 °C. Figure 1 pertains to **2**-MPC and illustrates the effect of increasing the S:Au ratio from 0.5:1 to 3:1, the average core diameter decreasing from 2.0 to 1.1 nm. The same two S:Au feed ratios were used in the syntheses of the other MPCs, and a summary of the core diameters is provided in Table 1. A similar relationship between the S:Au feed ratio and core diameter was previously pointed out by Hostetler et al. for alkane-coated MPCs.[35] The peptide MPCs appear to display smaller core dispersity and core size than are usually observed for alkanethiolate MPCs prepared under otherwise identical conditions.

Overall, the TEM data indicate that for both sets of experimental conditions d decreases for peptides capable of forming a helical secondary structure, i.e., with **1**−**3**. However, although some steric control of the growing-passivation competition during the reduction step can be inferred from literature data pertaining to poly(ethylene glycols)(PEG)[36] and alkanethiolates,[39] there is no perceptible similar trend in the **1**−**3** MPC series. The case of **2**-MPC obtained at a S:Au ratio of 3:1 is particularly interesting as the core diameter is only ∼1.1 nm, which is a value corresponding to nominal Au_{38} particles.[40] Such clusters were previously obtained by using alkanethiol or phenylethanethiol ligands.[28,41] The outcome observed with peptide **2** would thus provide an alternative way to obtain Au_{38} clusters. Because of the intrinsic relevance of this aspect, this and the other small peptide MPCs will be the specific subject of a forthcoming study.[42]

^{1}H NMR Spectrometry. The peptide MPCs were studied by ^{1}H NMR spectrometry. The data confirmed that the chemical integrity of the peptides is preserved upon MPC formation and that the signals are slightly sensitive to the distance of the protons from the gold cluster and the size of the latter, as already described for alkanethiolate MPCs.[35,43,44]

ROESY experiments were carried out for **2**-MPC in $CDCl_3$. As described for the free peptides, assignment of the proton resonances was based on the analysis of the $C^{\beta}H(i-1)\rightarrow NH(i)$ type and $NH(i)\rightarrow NH(i+1)$ type (Figure S6) through-space connectivities. The analysis indicates that also when assembled in the monolayer, the peptides adopt a prevailing folded structure in keeping with the pattern expected for the 3_{10}-helix. Noteworthy, we found that the signal of the amide N(1)H proton, 8.58 ppm, is downfield by 3 ppm with respect to the signal of the free peptide **2a**, 5.60 ppm (5 mM concentration). A smaller but still significant downfield shift was also observed for the N(2)H proton, the values being 7.14 and 6.35 ppm for **2**-MPC and **2a**, respectively. To further check whether the peptide behaves differently in the monolayer or in solution, we stepwisely added Me_2SO-d_6 to a **3**-MPC solution in $CDCl_3$. Compared to the spectrum of **3a** in $CDCl_3$, one of the NH protons shifts to a much higher value, 8.79 ppm (Figure 2). In analogy with the outcome of the ROESY experiments performed on **2**-MPC, this peak is attributed to the amide N(1)H and thus the shift also is on the order of 3 ppm (3.24 or 3.04 ppm, compared to the signals of 1 or 5 mM **3a**, respectively). A comparable shift (2.5 ppm) was reported for MPCs formed by amide-containing thiolate ligands in which the NH group is at similar distances from the gold core.[7b] Noteworthy, none of the peptide-MPC NH-proton chemical shifts is appreciably affected by Me_2SO-d_6 addition. Only the chemical shift of the N(1)H proton slightly decreases as the concentration of Me_2SO-d_6 increases above ∼7%; this shift, however, is opposite with respect to the trend already verified for the free peptide **3a**. First, we can conclude that Me_2SO-d_6 again fails to disrupt the

(39) Hicks, J. F.; Templeton, A. C.; Chen, S.; Sheran, K. M.; Jasti, R.; Murray, R. W.; Debord, J.; Schaaff, T. G.; Whetten, R. L. *Anal. Chem.* **1999**, *71*, 3703−3711.
(40) Häkkinen, H.; Barnett, R. N.; Landman, U. *Phys. Rev. Lett.* **1999**, *82*, 3264−3267.
(41) (a) Alvarez, M. M.; Khoury, J. T.; Schaaff, T. G.; Shafigullin, M. N.; Vezmar, I.; Whetten, R. L. *Chem. Phys. Lett.* **1997**, *266*, 91−98. (b) Schaaff, T. G.; Shafigullin, M. N.; Khoury, J. T.; Vezmar, I.; Whetten, R. L.; Cullen, W. G.; First, P. N.; Gutiérrez-Wing, C.; Ascensio, J.; Jose-Yacamán, M. J. *J. Phys. Chem. B* **1997**, *101*, 7885−7891. (c) Chen, S.; Ingram, R. S.; Hostetler, M. J.; Pietron, J. J.; Murray, R. W.; Schaaff, T. G.; Khoury, J. T.; Alvarez, M. M.; Whetten, R. L. *Science* **1998**, *280*, 2098−2101.
(42) Fabris, L.; Maran, F. Work in progress.
(43) Badia, A.; Lennox, R. B.; Reven, L. *Acc. Chem. Res.* **2000**, *33*, 475−481.
(44) Badia, A.; Gao, W.; Singh, S.; Demers, L.; Guccia, L.; Reven, L. *Langmuir* **1996**, *12*, 1262−1269.

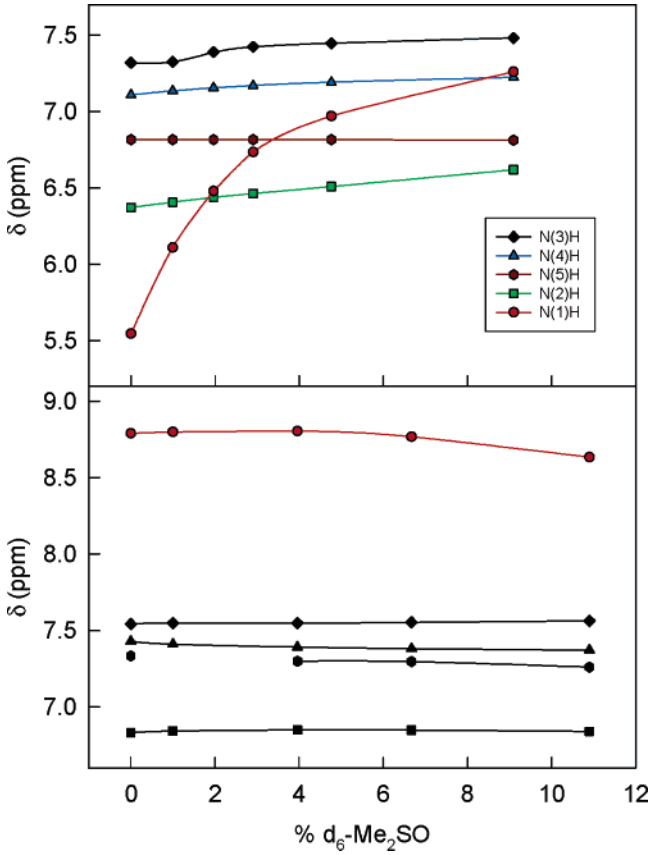

Figure 2. ^{1}H NMR titration in $CDCl_3$: Variation of the chemical shifts of the five amide protons of 1 mM **3a** (upper graph) and **3**-MPC (bottom graph) as a function of the addition of Me_2SO-d_6.

intrachain H-bonding network and thus the 3_{10}-helix secondary structure. The new aspect is the absence of the expected shift for the N(1)H proton: this may indicate that Me_2SO-d_6 is incapable of penetrating the inner part of the peptide monolayer or, if it does, it is incapable of interacting significantly with the otherwise free NH groups. This finding implies that the latter NH protons are involved in H-bonds with C═O groups of neighboring peptide chains, as similarly inferred for MPCs based on amide-containing thiolate ligands.[7b] The chemical shift of the amide N(2)H revealed by the ROESY experiments would suggest that this group also is involved in interligand interactions.

We should also mention that in CD_3OD solution the ^{1}H NMR spectrum of **3**-MPC is very similar, within a few tenths of ppm, to the pattern described for the $CDCl_3$/ Me_2SO-d_6 mixture; in particular, the N(1)H proton peak is at 8.52 ppm. This result also indicates that the H-bonding network involving the peptide NH groups in the monolayer is essentially unaffected by otherwise strongly interacting solvents. Finally, we observed that the chemical shift of the peak attributed to the N(1)H proton significantly increases with the peptide length: for the structured peptides, we measured ($CDCl_3$) 8.02 (**1**), 8.58 (**2**), and 8.79 ppm (**3**). Since a downfield shift is associated with an increase of hydrogen bonding, we may conclude that an increase of the peptide (intrachain) stiffness also optimizes the interligand network. As we will describe later, the presence of such complex H-bonding peptide network is fully supported by our IR absorption results.

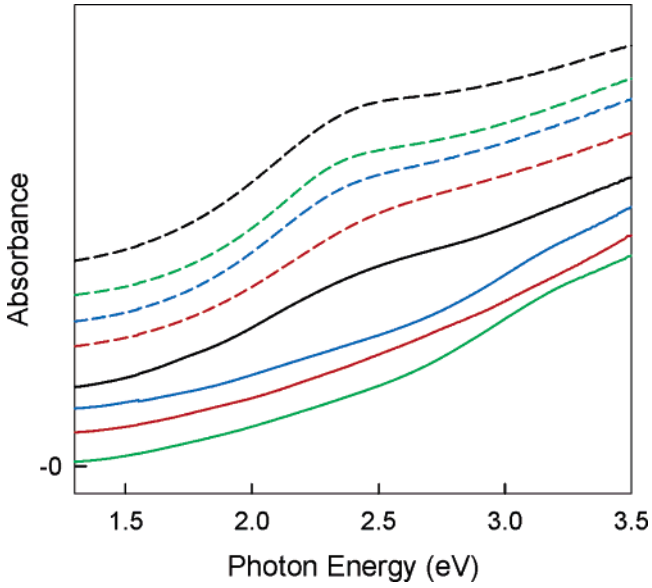

Figure 3. UV−vis absorption spectra of the peptide MPCs. The spectra were normalized to unity absorbance at 4 eV and displaced vertically for better viewing. The dashed lines correspond (top to bottom) to the 0.5:1 preparations and peptides **0**, **2**, **3**, and **1**; the solid lines (top to bottom) to the 3:1 preparations and peptides **0**, **3**, **1**, and **2**.

UV−Vis Spectroscopy. Optical absorption spectra provide information on the electronic structure of MPCs.[41b,45,46] Whetten and co-workers[45] described the evolution of the absorption spectra as a function of the core size of alkanethiolate MPCs. For sufficiently small particles (d < 1.7 nm) the absorption pattern is sensitive to the nature of monolayer, while it is largely independent of it for larger particles. As shown in Figure 3, only for the largest peptide MPCs there is a shoulder at 520 nm (2.38 eV), where the surface plasmon absorption of gold is expected to emerge as a true band exhibiting a maximum only for particles having diameters larger than ∼2.4 nm.[35,45] Independently of the ligand size, the shoulder fades away and eventually disappears for d < 1.6 nm.

The plots of the derivative of the absorbance (A) with respect to the photon energy near the plasmon band (Figure S5) allow one to better appreciate the dependence of the spectrum on the MPC size. In particular, we observed that at photon energies of 2.10 and 2.65 eV the spectra are particularly sensitive to the particle size. The values of the derivatives of the optical absorption with respect to the photon energy are plotted in Figure 4 as a function of the core diameters obtained from the TEM analysis. In the plot, we included one additional **1**-MPC obtained by carrying out the synthesis at an S:Au ratio slightly smaller than 0.5:1. The two solid lines mark quite satisfactorily the trends (r^2 = 0.968 and 0.926 for 2.65 and 2.10 eV, respectively), particularly if one takes into account the uncertainty associated with the TEM determinations. The d values calculated by using the two linear regressions are gathered in Table 1. Figure 4 would thus indicate that also for (related) peptide MPCs the optical size estimate may provide a useful

(45) Alvarez, M. M.; Khoury, J. T.; Schaaff, T. G.; Shafigullin, M. N.; Vezmar, I.; Whetten, R. L. *J. Phys. Chem. B* **1997**, *101*, 3706−3712.
(46) (a) Mie, G. *Ann. Phys.* **1908**, *25*, 377−445. (b) Kreibig, U.; Genzel, L. *Surf. Sci.* **1985**, *156*, 678−700. (c) Quinten, M.; Kreibig, U. *Surf. Sci.* **1986**, *172*, 557−577. (d) Barnett, R. N.; Cleveland, C. L.; Häkkinen, H.; Luedtke, W. D.; Yannouleas, C.; Landman, U. *Eur. Phys. J. D* **1999**, *9*, 95−104. (e) Kelly, K. L.; Coronado, E.; Zhao, L. L.; Schatz, G. C. *J. Phys. Chem. B* **2003**, *107*, 668−677.

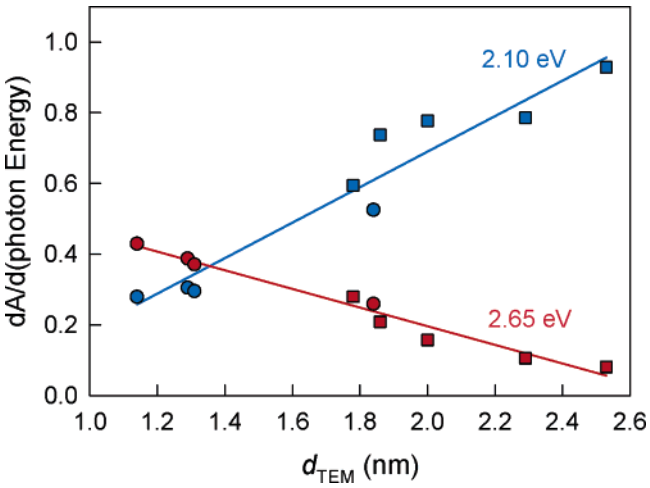

Figure 4. Plots of the derivatives of the UV−vis spectra calculated at photon energies of 2.10 (blue series) and 2.65 eV (red series) as a function of the cluster core diameter determined by TEM analysis. The circles pertain to the 3:1 series and the squares to the 0.5:1 series. The two solid lines are the corresponding linear fit to the data.

Table 2. TGA Data: Decomposition Temperature (Corresponding to a 5% Weight Loss) and Organic Weight Loss (wl%)

peptide	T_{dec} (0.5:1)	T_{dec} (3:1)	wl% (0.5:1)	wl% (3:1)
0	239.1	236.8	22.7	35.3
1	251.0	250.7	31.1	49.6
2	247.2	251.6	39.0	46.7
3	240.6	250.6	37.1	55.7

(and convenient) investigation tool, further stressing the importance of the optical absorption spectra to characterize small MPCs.[47] We should finally notice that for the smallest particle obtained some fine structure starts to be perceptible in the optical absorbance curve (Figure 3), but much less clearly as that displayed by Au_{38} clusters capped by alkanethiolate ligands.[28] This observation also would support the notion that the fine structure of the optical absorption spectra displayed by molecular-like MPCs may be affected by the capping ligand.[48]

Thermogravimetric Analysis and Monolayer Coverage. TGA[49] allows one to estimate the composition of the MPC. Previous TGA of gold nanoparticles protected by various types of thiolate ligand showed that the Au−S bond is broken at relatively high temperature (150−300 °C)[37,38,50,51] and the decomposition yields a metallic gold residue and volatile organic compounds, namely, the corresponding disulfides.[35] We verified the same outcome by IR absorption spectroscopy analysis of the organic vapors of **3**-MPC. The TGA was carried out on both series of peptide MPCs, and the results are summarized in Table 2. The decomposition temperature (T_{dec}), taken as the temperature corresponding to 5% weight loss, does not exhibit any significant dependency on the peptide length or the preparation procedure. This behavior is unusual because normally T_{dec} increases as the ligand molecular mass[51] increases.[9a,35,50] This is illustrated in Figure 5 for PEGs,[38] alkanethiols,[50] and arenethiols,[37a] also showing that ligands belonging to different families afford similar slopes. With all due caution associated with the complexity of TGA decomposition processes,[49] the pattern displayed by the peptide MPCs might be related to the peptide molecular dipole moment pointing its positive end toward the metal core and thus diminishing the charge density at sulfur (normally,[35,52] ca. −0.2). The observed TGA pattern would thus reflect a compensation between the increasing strength of the molecular dipole with the peptide length and the "normal" effect caused by increasing the molecular mass. The importance of the peptide dipole moment in affecting the MPC properties is supported by our recent data on its effect on the redox properties of small MPCs.[42]

Table 2 shows the weight losses measured by TGA for the investigated MPCs. By combining these data with the TEM diameters, the number of peptide ligands on each cluster can be calculated along with the ensuing surface coverage (θ = ratio of ligands to surface Au atoms) and peptide footprint. Concerning the number of Au atoms (N_{Au}), we may model the cluster as a sphere and calculate N_{Au} from the core diameters and the density of bulk fcc-Au (59 atoms/nm^3). Thus, by using the sphere model[50] and the TGA results, θ can be estimated. A different strategy is based on Au clusters whose sizes reflect a discrete sequence of fcc structures of truncated octahedral shape.[53] Each d value is associated with one of the "magic numbers" of Au atoms,[46d,53] allowing calculation of the Au mass pertaining to each cluster. By using the TGA weight loss, the number of ligands (N_L) is then estimated. The values of θ and of the peptide footprint are eventually obtained from the number of gold surface atoms.[35]

Analysis of our data shows that the polyhedron (Table 3) and sphere models (Supporting Information) yield comparable θ and N_L values; in the following, we make reference to the polyhedron model. For alkanethiolate ligands a θ value of ∼0.6 was calculated for ∼2 nm size clusters;[35,50] this value almost doubles the θ value of corresponding SAMs formed on extended gold surfaces, namely, 0.33.[54] In fact, the curvature of nanoclusters increases the monolayer packing with respect to flat gold surfaces, particularly for small particles and thanks to the presence of edges and vertexes.[55] Consequently, the alkanethiolate footprint has been reported to decrease from 0.22 to 0.15 nm^2 on going from 2D SAMs to MPCs of ca. 2.3 nm.[56] Because of the steric hindrance of the helical structure, a larger footprint is associated with the peptide ligands. In particular, we find that the 0.5:1 series, which also is characterized by MPCs of ∼2 nm, yields an average θ value of 0.43. For the smallest

(47) See also: Scaffardi, L. B.; Pellegri, N.; de Sanctis, O.; Tocho, J. O. *Nanotechnology* **2005**, *16*, 158−163.
(48) A similar quite featureless optical absorption behavior was observed by Chen and Kimura for gold MPCs having diameters in the range of 1.0−1.1 nm: Chen, S.; Kimura, K. *Langmuir* **1999**, *15*, 1075−1082.
(49) Wendlandt, W. W. M. *Thermal Analysis*, 3rd ed.; Wiley: New York, 1986.
(50) Terrill, R. H.; Postlethwaite, T. A.; Chen, C.-H.; Poon, C.-D.; Terzis, A.; Chen, A.; Hutchison, J. E.; Clark, M. R.; Wignall, G.; Londono, J. D.; Superfine, R.; Falvo, M.; Johnson, C. S., Jr.; Samulski, E. T.; Murray, R. W. *J. Am. Chem. Soc.* **1995**, *117*, 12537−12548.
(51) A similar pattern can be obtained from other literature MPC data: Foos, E. E.; Snow, A. W.; Twigg, M. E.; Ancona, M. G. *Chem. Mater.* **2002**, *14*, 2401−2408.
(52) Bourg, M. C.; Badia, A.; Lennox, R. B. *J. Phys. Chem. B* **2000**, *104*, 6562−6567.
(53) Whetten, R. L.; Khoury, J. T.; Alvarez, M. M.; Murthy, S.; Vezmar, L.; Wang, Z. L.; Stephens, P. W.; Cleveland, C. L.; Luedtke, W. D.; Landman, U. *Adv. Mater.* **1996**, *8*, 428−432.
(54) (a) Widrig, C. A.; Alves, C. A.; Porter, M. D. *J. Am. Chem. Soc.* **1991**, *113*, 2805−2810. (b) Kim, Y.-T.; McCarley, R. L.; Bard, A. J. *J. Phys. Chem.* **1992**, *96*, 7416−7421.
(55) (a) Luedtke, W. D.; Landman, U. *J. Phys. Chem.* **1996**, *100*, 13323−13329. (b) Badia, A.; Cuccia, L.; Demers, L.; Morin, F.; Lennox, R. B. *J. Am. Chem. Soc.* **1997**, *119*, 2682−2692.
(56) (a) Camillone, N., III; Chidsey, C. E. D.; Lui, G.-Y.; Scoles, G. *J. Chem. Phys.* **1993**, *98*, 4234−4245. (b) Sellers, H.; Ulman, A.; Schnidman, Y.; Eilers, J. E. *J. Am. Chem. Soc.* **1993**, *115*, 9389−9401. (c) Badia, A.; Singh, S.; Demers, L.; Cuccia, L.; Brown, G. R.; Lennox, R. B. *Chem. Eur. J.* **1996**, *2*, 359−363.

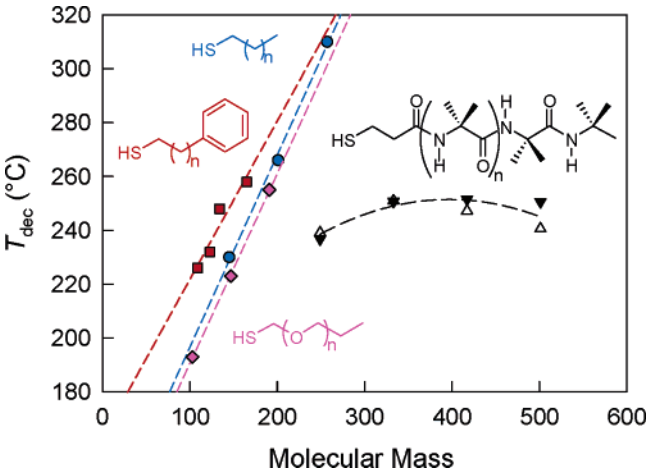

Figure 5. Plots of the MPC decomposition temperature versus the ligand molecular weight for the 0.5:1 (▼) and 3:1 (△) peptide MPCs, PEGs[38] (◆), alkanethiols[50] (●), and arenethiols[37a] (■).

Table 3. Surface Coverage, Number of Peptide Ligands, and Peptide Footprints (MPC Surface Area over the Number of Ligands) from TEM and TGA Data and Using the Polyhedron Model

peptide	S:Au	d_{TEM} (nm)	N_{Au}	θ	N_L	footprint (nm^2)
0	0.5:1	2.3	309	0.45	73	0.27
1		1.8	201	0.42	54	0.28
2		2.0	225	0.49	68	0.22
3		1.9	225	0.37	52	0.29
0	3:1	1.8	201	0.69	88	0.17
1		1.3	55	0.77	32	0.20
2		1.1	38	0.47	16	0.29
3		1.3	55	0.65	27	0.24

particles, obtained in the 3:1 preparations, a larger average θ is calculated; namely, $\theta \sim 0.65$. A similar relative variation is observed for alkanethiolate and phenyethanethiolate MPCs for which θ increases to 0.75 when the core diameter is reduced to 1.1 nm.[28]

If the peptide helix is approximated, using molecular models, as a cylinder, a footprint of 0.64 nm^2 can be calculated. This estimate pertains to the theoretical footprint on a flat surface. On the other hand, from the N_L and core-size values of Table 3, we calculated the peptide-helix footprints to be in the range of 0.17−0.29 nm^2. The smaller experimental footprint values clearly indicate that these peptides are extremely well-packed in the monolayer. The reasons for this behavior can be related to the radial distribution of the ligands on the small gold clusters and the fact that our peptides are rather thin near the gold surface because of the -S−CH_2−CH_2- groups. That the core size matters is also supported by a comparison with very recent literature data pertaining to much larger gold nanoparticles (d = 12.3 nm) capped by peptides of similar sizes and for which an experimental footprint of 0.55 nm^2 could be estimated.[10b]

Finally, the results pertaining to both the 3:1 and 0.5:1 series were compared with the results reported for alkanethiolate MPCs. We calculated that the peptide surface coverage is, on the average, smaller by 15−25% relative to the thinner alkanethiolate ligand monolayers (polyhedron model). For example, if we focus on the largest and the smallest clusters prepared, the experimental MPC formulas (average of the two models) are $Au_{38}Pep_{18}$ and $Au_{309}Pep_{80}$ as opposed to (filled alkanethiolate shell) $Au_{38}L_{24}$[28] and $Au_{309}L_{98}$,[37a] respectively.

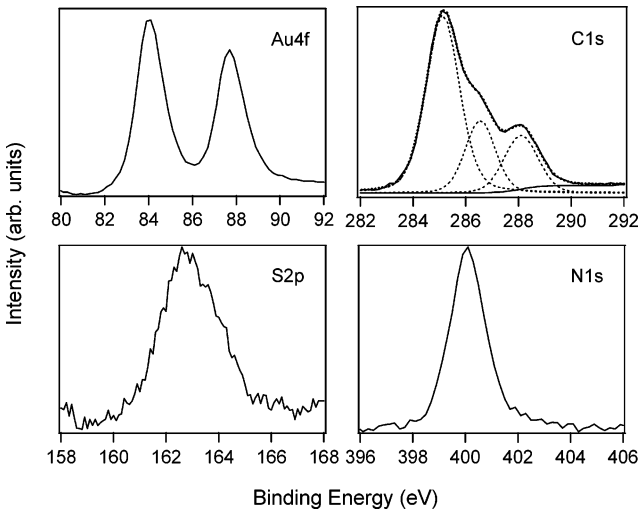

Figure 6. XPS spectra in the Au4f, C1s, S2p, and N1s regions for **3**-MPC (0.5:1 preparation). The C1s signal has been deconvoluted into the three components of the carbon types of the peptide ligands.

Table 4. Binding Energy (eV) and Number of Peptide Ligands per Cluster Au Atoms

MPC	$Au4f_{7/2}$	O1s	N1s	S2p	S:Au	S:Au[a]
3, 0.5:1	84.0	531.7	400.0	162.6	0.32	0.23
2, 0.5:1	84.0	532.4	399.9	162.8	0.33	0.30
0, 0.5:1	84.0	532.6	400.0	162.6	0.28	0.24
2, 3:1	84.2	532.0	399.8	163.0	0.44	0.42

[a] From TGA data, using the TEM diameters and the polyhedron model.

X-ray Photoelectron Spectroscopy. We carried out the XPS analysis on four MPC samples: three of them were taken from the 0.5:1 series, chosen to test the ligand effect on particles (the MPCs of **0**, **2**, and **3**) having comparable sizes, and the last sample served to test the effect of decreasing the particle size (from 2.0 to 1.1 nm), while keeping the peptide ligand, **2**, constant. Figure 6 illustrates spectral regions pertaining to the XPS analysis of **3**-MPC. For all samples, we obtained signals from gold, carbon, oxygen, nitrogen, and sulfur; no other elements were detected. The Au4f level is characterized by a sharp doublet having a peak-to-peak separation of 3.6 eV and a full width at half-maximum (fwhm) of 1.6 eV.

Within the 0.5:1 MPC series, the binding energy (BE) of the $Au4f_{7/2}$ peak (Table 4) is constant to 84.0 eV, which is the typical value expected when thiolate monolayers self-assemble onto gold nanoclusters or extended gold surfaces.[35,52,57] Only for the small **2**-MPC a shift to a higher BE is perceptible, as expected for molecular-like MPCs.[35,58] The C1s band is broad due to the presence of three components: methyl and methylene carbon, C−N type carbon, and carbonyl carbon. Deconvolution of this peak (Figure 6) allows determination of the corresponding BEs. For **3**-MPC we obtained, e.g., 285.0 eV (fwhm, 1.5 eV), 286.5 eV (fwhm, 1.4 eV), and 288.1 eV (fwhm, 1.5 eV), respectively. Such values are in very good agreement with the XPS analysis of methylene-chain carbons,[59] amide-containing thiolates,[5k,60] and 2D SAMs composed by similar Aib-based

(57) (a) van der Putten, D.; Zanoni, R.; Coluzza, C.; Schmid, G. *J. Chem. Soc., Dalton Trans.* **1996**, 1721−1725. (b) Heister, K.; Zharnikov, M.; Grunze, M.; Johansson, L. S. O. *J. Phys. Chem. B* **2001**, *105*, 4058−4061. (c) Joseph, Y.; Besnard, I.; Rosenberger, M.; Guse, B.; Nothofer, H.-G.; Wessels, J. M.; Wild, U.; Knop-Gericke, A.; Su, D.; Schlögl, R.; Yasuda, A.; Vossmeyer, T. *J. Phys. Chem. B* **2003**, *107*, 7406−7413.
(58) Zhang, P.; Sham, T. K. *Phys. Rev. Lett.* **2003**, *90*, 245502−1−245502−4.

thiolated peptides.[6] The BEs pertaining to the O1s peaks agree well with previous observations for peptide or amide C═O oxygen signals, which are in the range 531−533 eV.[5b,d,e,k,p,61] The N1s peak also has the BE value expected for amide groups, within experimental uncertainty. The intensity of the S2p region is very low because of the tiny amount of sulfur in the samples. Nonetheless, we could observe that the S2p BE values are somewhat larger than the value of ∼162 eV typical of thiols strongly interacting with gold in 2D and 3D SAMs,[5k,p,35,52,57c,60c,62] but still significantly smaller than those found for free thiols and elemental sulfur (163.5−164.2 eV).[52,59a,62b,63] In addition, the BE appears to increase as the MPC size decreases. By using the approach described by Lennox and co-workers,[52] based on a correlation between the $S2p_{3/2}$ binding energy and the charge density on the S atom,[64] we estimate a lower and a maximum charge of −0.17 and −0.09, which should be compared with the charge generally estimated for alkanethiolates, −0.2.[52] The difference would be in keeping with the effect brought about by the peptide dipole moment.

The final issue stemming from the XPS data concerns the elemental analysis. Reference was made to nitrogen, which is almost unaffected by adventitious environmental contamination. For **3**-MPC (the longer the peptide, the more precise is the calculation), we found the following theoretical and experimental ratios (C,N,O,S): 4.6, 1, 1, 0.2 and 5.1, 1, 0.95, 0.15. In addition, whereas the relative amounts of the different carbon species determined by deconvolution of the XPS signal are 60% (methyl and methylene carbon), 21% (C−N type-carbon), and 19% (carbonyl carbon), the corresponding theoretical values are 57, 22, and 22%. The good agreement thus ensures that the integrity of the peptide ligand is preserved in the MPC. Similar results are found for the other MPCs. The second analysis is about N_L per cluster gold atoms, which is easily calculated from the S:Au ratios (sixth column of Table 4). These ratios can be compared with the corresponding data (last column) stemming from TGA: overall, the agreement between the two sets of data is satisfactory, the average uncertainty being ∼15%. The very good agreement between the S:Au data of the last entry is particularly worth noting, and this further supports the notion that the **2**-MPC obtained in the 3:1 preparation is particularly small.

IR Absorption Spectroscopy. Vibrational spectroscopy has been used occasionally to study MPCs but proved to be a powerful tool to characterize the structure and orientation of 3D SAMs.[7,35,65] We already discussed the IR absorption behavior of the free ligands and particularly how the N−H stretch region (amide A) allows one to distinguish the amide protons that are involved in C═O···H−N hydrogen bonds from those that are not. The spectra obtained in the N−H stretch region with the two series of MPCs are shown in Figure 7 (graphs *b* and *c*) together with those recorded for the trityl precursors **0a**−**3a** (graph *a*) in the same solvent (CH_2Cl_2). The latter series clearly shows that the onset of intramolecular C═O···H−N hydrogen bonding is significantly evident starting from **1a**. It also shows that while the frequency of the band corresponding to the two free N−H groups does not change (3421 ± 1 cm^{-1}), the frequency of the N−H band of intramolecularly H-bonded peptides decreases as the peptide length

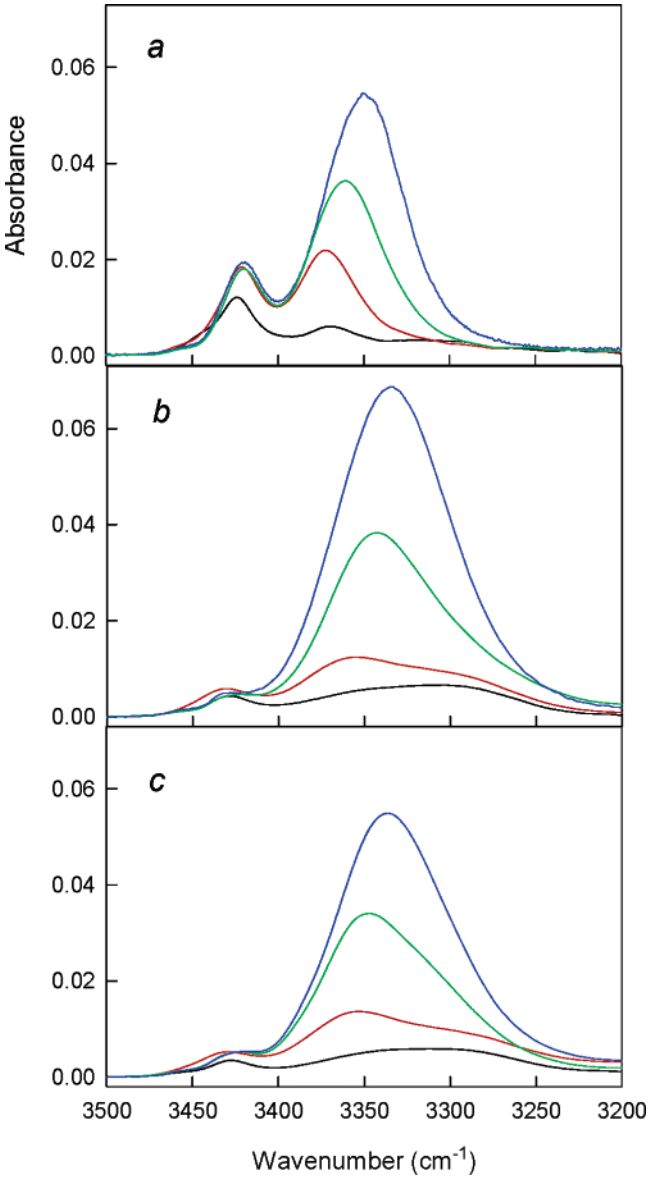

Figure 7. FT-IR absorption spectra for the N−H stretch region of peptides **0a**−**3a** (graph *a*), 0.5:1 MPCs (graph *b*), and 3:1 MPCs (graph *c*). The spectra correspond (bottom to top) to **0** (black), **1** (red), **2** (green), and **3** (blue). The spectra were acquired in CH_2Cl_2 solutions, and the absorbance was corrected for the peptide concentration.

(59) (a) Bain, C. D.; Blebuyck, H. A.; Whitesides, G. M. *Langmuir* **1989**, *5*, 723−727. (b) Laibinis, P. E.; Whitesides, G. M.; Allara, D. L.; Tao, Y.-T.; Parikh, A. N.; Nuzzo, R. G. *J. Am. Chem. Soc.* **1991**, *113*, 7152−7167.
(60) (a) Beamson, G.; Briggs, D. *High-Resolution XPS of Organic Polymers*: Wiley: Chichester, U.K., 1992. (b) Uvdal, K.; Bodö, P.; Liedberg, B. *J. Colloid Interface Sci.* **1992**, *149*, 162−173. (c) Cavalleri, O.; Oliveri, L.; Daccà, A.; Parodi, R.; Rolandi, R. *Appl. Surf. Sci.* **2001**, *175*−*176*, 357−362.
(61) (a) Clark, D. T.; Peeling, J.; Colling, L. *Biochim. Biophys. Acta* **1976**, *453*, 533−545. (b) Bomben, K. D.; Dev, S. B. *Anal. Chem.* **1988**, *60*, 1393−1397. (c) Petoral, R. M., Jr.; Uvdal, K. *J. Electron Spectrosc. Relat. Phenom.* **2003**, *128*, 159−164.
(62) (a) Ishida, T.; Choi, N.; Mizutani, W.; Tokumoto, H.; Kojima, I.; Azehara, H.; Hokari, H.; Akiba, U.; Fujihira, M. *Langmuir* **1999**, *15*, 6799−6806. (b) Castner, D. G.; Hinds, K.; Grainger, D. W. *Langmuir* **1996**, *12*, 5083−5086. (c) Maye, M. M.; Luo, J.; Lin, Y.; Engelhard, M. H.; Hepel, M.; Zhong, C.-J. *Langmuir* **2003**, *19*, 125−131.
(63) (a) Riga, J.; Verbist, J. J. *J. Chem. Soc., Perkin Trans. 2* **1983**, 1545−1551. (b) Nuzzo, R. G.; Zegarski, B. R.; Dubois, L. H. *J. Am. Chem. Soc.* **1987**, *109*, 733−740. (c) Moulder, J. F.; Stickle, W. F.; Sobol, P. W.; Bomben, K. D. *Handbook of X-ray Photoelectron Spectroscopy*; Perkin-Elmer: Eden Prairie, MN, 1992.
(64) Lindberg, B. J.; Hamrin, K.; Johansson, G.; Gelius, U.; Fahlman, A.; Nordling, C.; Siegbahn, K. *Phys. Scr.* **1970**, *1*, 286−298.
(65) (a) Templeton, A. C.; Hostetler, M. J.; Kraft, C. T.; Murray, R. W. *J. Am. Chem. Soc.* **1998**, *120*, 1906−1911. (b) Paulini, R.; Frankamp, B. L.; Rotello, V. M. *Langmuir* **2002**, *18*, 2368−2373.

increases. This decrease is related to the peptide stiffness and thus to the extent of intramolecular H-bond formation.

To better appreciate the relative similarities and differences, also in terms of absorbance maxima, we normalized the MPC spectra of Figure 7 by taking into account the actual number of peptides per particle as obtained from TGA. The absorption values of Figure 7 thus reflect our best estimate of the peptide concentration, whether corresponding to an actual molar concentration (1 mM) or to the same concentration calculated as if the peptides forming the monolayer were free diffusing species. Graphs *b* and *c* of Figure 7, which correspond to the 0.5:1 and 3:1 series, respectively, are qualitatively very similar but also significantly differ from those of the free ligands. First, the band intensity of the free N−H groups of the MPCs of **0**−**3** (at 3433 ± 1 cm^{-1}) is only about one-fourth of that recorded for **1a**−**3a**. Second, starting from the shortest ligand an absorption band appears at low frequencies; this band is roughly constant (from derivative analysis of the absorption spectra—not shown) in terms of both position (3287 ± 5 cm^{-1}) and intensity. Third, the intensity of the band at intermediate frequencies is an increasing function of the peptide length. As the length increases, the frequency undergoes the same red shift observed for the free peptide, although the values are on the average lower by 8 cm^{-1}. The frequency shift and the intensity increase eventually causes this band to overlap the above-mentioned low-energy band, thus making the resulting band quite broad. Whereas the vibrational mode observed at intermediate frequencies is assigned to the intrachain C═O···H−N hydrogen bonds, the low-frequency component is attributed to the N−H groups that are hydrogen-bonded to neighbor peptides. In fact, the observed frequencies are close to the values expected for such interactions, for example as found with β-sheets[66] or for MPCs with embedded amide groups.[5d,e,7b] Close inspection of the graphs *b* and *c* shows that the intensity of the main N−H band of the 0.5:1 MPC preparation series is, overall, slightly larger than that of the 3:1 series. The reason for such a trend may be related to the size of the 0.5:1 MPCs, which are substantially larger than the corresponding 3:1 MPCs and are thus characterized by the presence of flatter surfaces. Thus, the band intensity may be related to the surface selection rules, according to which the absorbance of bands with a transition moment essentially perpendicular to the surface are expected to appear with enhanced intensities.[67] The phenomenon is expected to be more evident when the monolayer forms on a flatter surface. In this framework, the above observation would thus support the notion that the peptides are assembled by directing their main axis (and thus, according to the 3_{10}-helical structure, the intrachain hydrogen-bonded C═O and N−H groups) essentially perpendicular to the surface.

Information on peptide conformation is also found in the amide I and amide II regions. Although the fine structure of these bands is quite complex,[33] we now will focus only on relative comparisons. For amide I, which corresponds to the C═O stretch and for fully stable 3_{10}-helices occurs at 1662−1666 cm^{-1}, the main difference between precursors **0a**−**3a** and corresponding MPCs (Figure 8: once again, the absorption values were normalized for the actual peptide concentration) is that the latter systems exhibit lower frequencies (typically, by

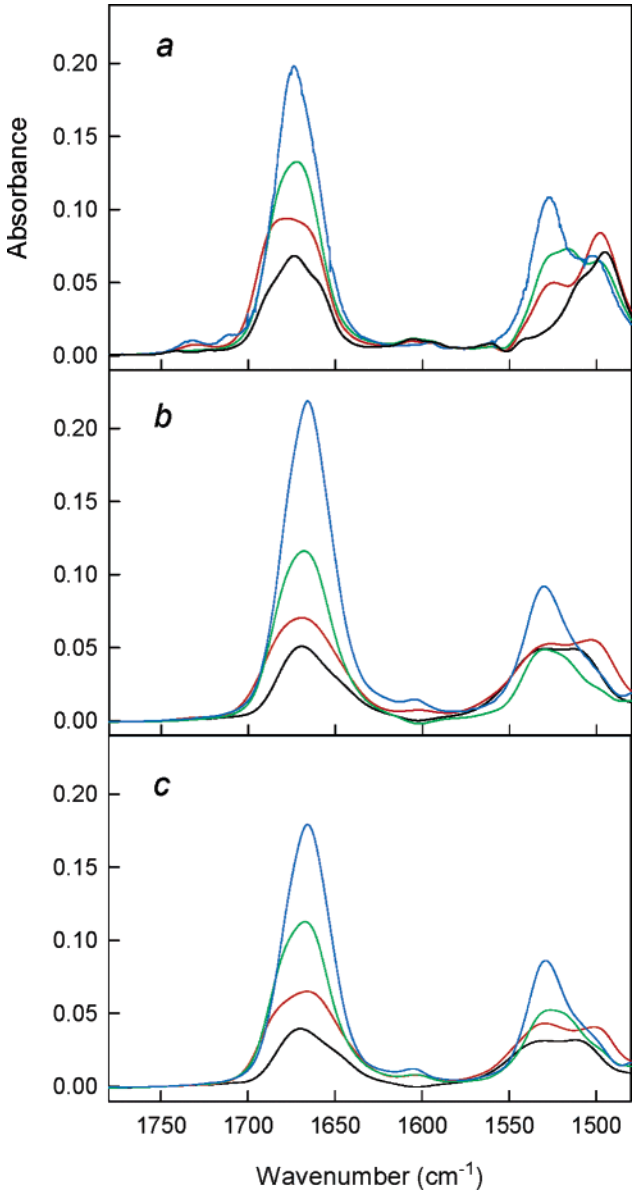

Figure 8. FT-IR absorption spectra for the amide I and amide II regions of peptides **0a**−**3a** (graph *a*), 0.5:1 MPCs (graph *b*), and 3:1 MPCs (graph *c*). The spectra correspond (bottom to top) to **0** (black), **1** (red), **2** (green), and **3** (blue). The spectra were acquired in CH_2Cl_2 solutions, and the absorbance was corrected for the peptide concentration.

~8 cm^{-1}). The spectral region pertaining to the amide II band (for fully formed 3_{10}-helices the amide II band is expected at 1531−1533 cm^{-1})[68] is complex because the peptides that we investigated are short oligomers. We can note, however, the tendency to develop a well-defined amide II band as we move from **0a** to **3a**. Interestingly, the corresponding MPCs display this tendency even more promptly, which suggests that the system now is stiffer (more stable 3_{10}-helices for peptides buried in the monolayer). We note also that, compared to the free peptides, the directions of the shifts of the amide I and the amide II bands are different: for example, the values shown by peptide **3** are 1674 and 1666 cm^{-1} (amide I) and 1526 and 1530 cm^{-1} (amide II). These shifts are associated with chemisorption to

(66) Toniolo, C.; Palumbo, M. *Biopolymers* **1977**, *16*, 219−224.
(67) Greenler, R. G. *J. Chem. Phys.* **1966**, *44*, 310−315.

(68) A similar enhancement could be observed for a 2D-SAM formed by an Aib-containing hexapeptide.[6]

the gold surface and thus to the interactions between the peptides in the adsorbed layer, as also noticed for peptide 2D SAMs.[5b] The relative absorption intensities of the amide I and the amide II bands is particularly worth noting: the intensity ratio (amide I to amide II absorbance) increases from 1.82 to 2.08 to 2.37 (peptide **3**) as we go from the free ligand to the 3:1 MPCs and finally to the 0.5:1 MPCs, respectively. This comparison also supports the view that the peptides (and thus the intrachain C═O···H−N hydrogen bonds) are oriented (mostly) perpendicular to the surface, thereby experiencing a surface enhancement for the amide I (and amide A) vibrational mode.[68]

As final experimental notes, we mention that the IR absorption behavior of the free ligand in solution is rather different from that obtained in a KBr pellet, where the peptides are packed favoring the formation of interligand C═O···H−N hydrogen bonds. In particular, whereas in KBr the amide I band shifts to smaller energies, the amide II experiences the opposite trend. On the other hand, almost no difference is observed (Figure S2) for the MPCs, in keeping with the notion that when the peptides are buried in the monolayer they feel no difference whether the MPC is in solution. We also carried out IR absorption experiments (with **3**-MPC and **3a**: see Supporting Information, Figures S3 and S4) in acetonitrile, which is a solvent prone to interact by hydrogen bonding with free NH groups. Remarkably, we did not notice any significant difference (both in the amide A and the amide I and II regions) with respect to the results obtained in CH_2Cl_2, while the effect is evident with the free ligand. These results also support the view that the properties of the peptide monolayer are not affected by exogenous species, as already discussed for the NMR results (Me_2SO-d_6 titrations).

The above IR absorption data and comparisons indicate that the peptides are both intraligand (according to the 3_{10}-helical structure) and interligand hydrogen-bonded. The latter interaction should involve the first two N−H groups, which are not involved in intrachain interactions. This conclusion also implies that neighbor peptide adsorbates should provide C═O groups that are already involved in intrachain C═O···H−N hydrogen bonds. These three-center hydrogen bonds allow formation of a strong interchain bonding network and, since they are embedded inside the monolayer, they are largely unaffected by an increase of the peptide length.

Conclusions

We have prepared a series of gold nanoclusters in which the capping monolayer is composed by thiolated peptide ligands. The peptides are oligomers based on the Aib unit and were chosen for their propensity to promptly form 3_{10}-helical structures. The corresponding MPCs were prepared under different experimental conditions and characterized with various physicochemical tools. The core diameters of the MPCs are smaller when more structured peptides are used (i.e., **1**−**3**), which would suggest that sterically hindered and conformationally constrained peptide ligands are better suited to passivate the cluster growth at an earlier stage of its formation. The clusters prepared by using a 3:1 S:Au ratio and structured peptides (**1**−**3**) are particularly small, being in the 1.1−1.3 nm range.

The structural integrity of the peptides in the monolayer was assessed. The data indicate that the peptides are remarkably well-packed in the monolayer and that the surface coverage is typically 75−85% the value calculated for alkanethiolate MPCs of similar sizes. Spectral analyses indicate that the secondary structure does not change when the peptide is in the monolayer and that H-bond acceptors do not alter the H-bond interactions. The results also provide evidence for the presence of interligand C═O···H−N hydrogen bonds in the MPCs and suggest that the peptides are mostly oriented perpendicular to the gold surface. The peptide secondary structure and the interligand H-bonding network are envisaged as responsible for the successful preparation of this new class of small MPCs. For future applications, the rigidity of these peptide monolayers could be employed to control the relative distance and thus the physicochemical behavior of electro- or photoactive groups attached on the MPC periphery.

Acknowledgment. This work was financially supported by the Ministero dell'Istruzione, dell'Università e della Ricerca (MIUR) and the National Consortium of Materials Science and Technology (INSTM). S.A. and L.F. also acknowledge a grant from the Università di Padova (Progetto Giovani Ricercatori). We thank Dr. G. Pace for the TGA.

Supporting Information Available: Additional preparation and characterization data of peptides and MPCs. This material is available free of charge via the Internet at http://pubs.acs.org.

JA0560581